

Testing and analysis of high frequency electroelastic characteristics of piezoelectric transformers

F. NARITA, Y. SHINDO, F. SAITO, M. MIKAMI

*Department of Materials Processing
Graduate School of Engineering
Tohoku University
Aoba-yama, 6-6-02, Sendai 980-8579, Japan*

THIS ARTICLE PRESENTS the results of experimental and numerical work on the dynamic electroelastic response of Rosen-type piezoelectric transformers. Experiments were conducted to measure the electrical impedance, phase angle and voltage gain at various frequencies. The three-dimensional finite element method was also employed to solve the coupled electro-elastic boundary value problem. The electrical impedance, phase angle and voltage gain were calculated and a comparison was made between experiment and simulation. The effects of load resistance and capacitance on the voltage gain and electroelastic field concentrations were also discussed in detail.

Key words: piezoelectric material systems, dynamic electroelastic field concentrations, transformer.

1. Introduction

PIEZOELECTRIC CERAMICS are characterized as smart materials and structures, and have been widely used in the area of sensors and actuators. The principle of operation of a piezoelectric transformer is a combined function of sensors and actuators, so that energy can be transformed from electrical form to electrical form via mechanical vibration. Small electronic devices which operate at high voltages require a compact transformer to step up the low voltage of available power supplies, and the piezoelectric transformers find extensive applications in the liquid crystal display backlight inverter to reduce the height and size of the notebook computers, personal digital assistants, digital video cameras, etc. The piezoelectric transformers have several inherent advantages [1, 2] over electromagnetic transformers such as low cost, high efficiency, compact size, and no magnetic noise. Recently, HWANG *et al.* [3] measured the electrical characteristics for Rosen-type piezoelectric transformers using PNW-PMN-PZT composition, and discussed the effect of load resistance on the output voltage and current of the piezoelectric transformers. KARLASH [4] considered the forced vibrations of the Rosen-type piezoelectric transformers and analyzed the frequency prop-

erties and stress state of the transformer using one-dimensional approximation. NARITA *et al.* [5] solved the plane strain electroelastic problem of a central active piezoelectric transformer in presence of a crack located normally to the interfaces, and discussed the effect of electric field on the fracture mechanics parameters such as stress intensity factor, energy release rate and energy density factor.

When the piezoelectric transformers are operated, the piezoelectric ceramics will be in mechanical resonance and large electroelastic fields will appear in the piezoelectric ceramics. Prediction of the intensified fields in the vicinity of an electrode tip or possibly a crack tip would most likely require detailed finite element calculations. A two or three-dimensional finite element model of piezoelectric materials and devices with cracks [6, 7] or electrodes [8, 9] under direct current (DC) electric fields was developed, and numerical simulation results were shown to be in qualitative agreement with the test data. Finite element analysis was also presented to study the nonlinear behavior due to domain wall motion in piezoelectric devices under alternating current (AC) electric fields, and a comparison was made between numerical results and experimental data [10].

In this paper, we experimentally and numerically investigate the high-frequency characteristics in Rosen-type piezoelectric transformers. The electrical impedance, phase angle and voltage gain are measured. Three-dimensional finite element simulations are then done to predict the electrical impedance, phase angle and voltage gain, and results produced by the model are compared with experimental values. The internal electroelastic fields are also calculated and the results are presented graphically.

2. Experimental procedure

The transformers were fabricated using a hard-lead zirconate titanate (PZT) C-205. The material characteristics are listed in Table 1 (Fuji Ceramics Co., Ltd., Japan). The specimen used is a Rosen-type structure (Fig. 1). The input half of the transformer is poled along its thickness while the output half is poled along its length. All external faces are free. The transformer has a length of 50 mm, a width of 13 mm and a thickness of 2 mm.

Table 1. Material properties of C-205.

	Elastic stiffnesses					Piezoelectric coefficients			Dielectric constants		Mass density
	c_{11}	c_{33}	c_{44}	c_{12}	c_{13}	e_{31}	e_{33}	e_{15}	ϵ_{11}	ϵ_{33}	ρ
	$(\times 10^{10} \text{ N/m}^2)$					(C/m^2)			$(\times 10^{-10} \text{ C/Vm})$		(kg/m^3)
C-205	15.11	8.43	8.70	13.22	2.76	-4.26	18.52	13.59	79.47	68.68	7800

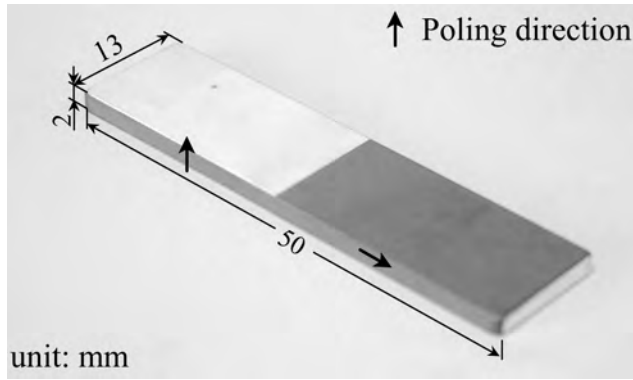


FIG. 1. Rosen-type transformer.

Figure 2 shows the driving circuits of the specimen. The transformer was driven by an AC voltage V_{in} using a function generator. Input and output resonant frequencies were measured by using an impedance/phase analyzer, as shown in Figs. 2 (a) and 2 (b), respectively. Voltage gain V_{out} was also measured by a digital multimeter (See Fig. 2 (c)). Load resistance and capacitance of the digital multimeter are $R = 1\text{ M}\Omega$ and $C = 160\text{ pF}$, respectively.

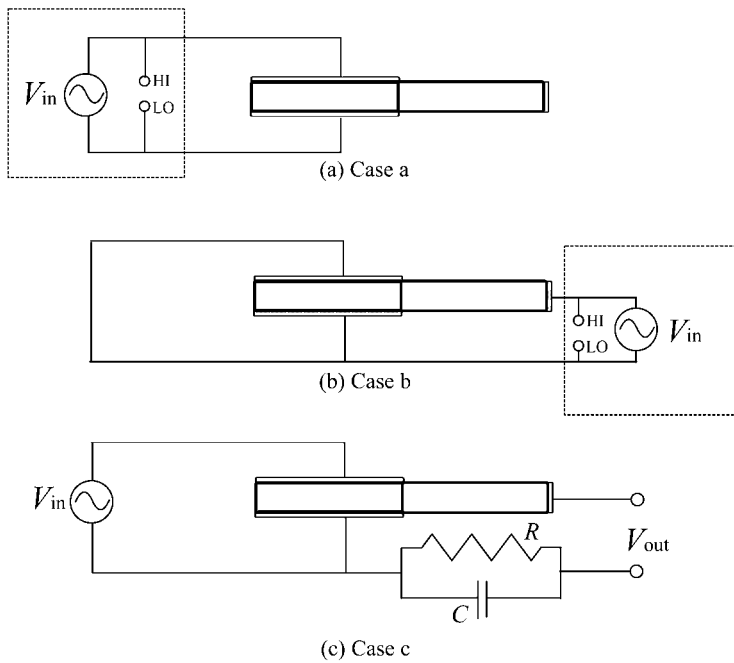


FIG. 2. Test circuits of the transformer.

3. Finite element analysis

3.1. Basic equations

Consider a linear piezoelectric material with no body force and free charge. The governing equations in the Cartesian coordinates x_i ($i = 1, 2, 3$) are given by

$$(3.1) \quad \sigma_{ji,j} = \rho u_{i,tt},$$

$$(3.2) \quad D_{i,i} = 0,$$

where σ_{ij} is the stress tensor, D_i is the electric displacement vector, u_i is the displacement vector, ρ is the mass density, a comma denotes partial differentiation with respect to the coordinate x_i or the time t , and the Einstein summation convention over repeated indices is used. The relation between the strain tensor ε_{ij} and the displacement vector u_i is given by

$$(3.3) \quad \varepsilon_{ij} = \frac{1}{2}(u_{j,i} + u_{i,j})$$

and the electric field intensity is

$$(3.4) \quad E_i = -\phi_{,i},$$

where ϕ is the electric potential. Constitutive relationships are

$$(3.5) \quad \sigma_{ij} = c_{ijkl}\varepsilon_{kl} - e_{kij}E_k,$$

$$(3.6) \quad D_i = e_{ikl}\varepsilon_{kl} + \epsilon_{ik}E_k,$$

where c_{ijkl} is the elastic constant, e_{ikl} is the piezoelectric constant, ϵ_{ik} is the dielectric permittivity, and

$$(3.7) \quad c_{ijkl} = c_{jikl} = c_{ijlk} = c_{jilk} = c_{klij}, \quad e_{kij} = e_{kji}, \quad \epsilon_{ik} = \epsilon_{ki}.$$

For piezoelectric ceramics which exhibit symmetry of a hexagonal crystal of class 6 mm with respect to principal axes x_1, x_2 , and x_3 , the constitutive relations can be written in the following form:

$$(3.8) \quad \begin{Bmatrix} \sigma_1 \\ \sigma_2 \\ \sigma_3 \\ \sigma_4 \\ \sigma_5 \\ \sigma_6 \end{Bmatrix} = \begin{bmatrix} c_{11} & c_{12} & c_{13} & 0 & 0 & 0 \\ c_{12} & c_{11} & c_{13} & 0 & 0 & 0 \\ c_{13} & c_{13} & c_{33} & 0 & 0 & 0 \\ 0 & 0 & 0 & c_{44} & 0 & 0 \\ 0 & 0 & 0 & 0 & c_{44} & 0 \\ 0 & 0 & 0 & 0 & 0 & c_{66} \end{bmatrix} \begin{Bmatrix} \varepsilon_1 \\ \varepsilon_2 \\ \varepsilon_3 \\ \varepsilon_4 \\ \varepsilon_5 \\ \varepsilon_6 \end{Bmatrix} - \begin{bmatrix} 0 & 0 & e_{31} \\ 0 & 0 & e_{31} \\ 0 & 0 & e_{33} \\ 0 & e_{15} & 0 \\ e_{15} & 0 & 0 \\ 0 & 0 & 0 \end{bmatrix} \begin{Bmatrix} E_1 \\ E_2 \\ E_3 \end{Bmatrix},$$

$$(3.9) \quad \begin{Bmatrix} D_1 \\ D_2 \\ D_3 \end{Bmatrix} = \begin{bmatrix} 0 & 0 & 0 & 0 & e_{15} & 0 \\ 0 & 0 & 0 & e_{15} & 0 & 0 \\ e_{31} & e_{31} & e_{33} & 0 & 0 & 0 \end{bmatrix} \begin{Bmatrix} \varepsilon_1 \\ \varepsilon_2 \\ \varepsilon_3 \\ \varepsilon_4 \\ \varepsilon_5 \\ \varepsilon_6 \end{Bmatrix} + \begin{bmatrix} \epsilon_{11} & 0 & 0 \\ 0 & \epsilon_{11} & 0 \\ 0 & 0 & \epsilon_{33} \end{bmatrix} \begin{Bmatrix} E_1 \\ E_2 \\ E_3 \end{Bmatrix},$$

where

$$(3.10) \quad \begin{aligned} \sigma_1 &= \sigma_{11}, & \sigma_2 &= \sigma_{22}, & \sigma_3 &= \sigma_{33}, \\ \sigma_4 &= \sigma_{23} = \sigma_{32}, & \sigma_5 &= \sigma_{31} = \sigma_{13}, & \sigma_6 &= \sigma_{12} = \sigma_{21}, \end{aligned}$$

$$(3.11) \quad \begin{aligned} \varepsilon_1 &= \varepsilon_{11}, & \varepsilon_2 &= \varepsilon_{22}, & \varepsilon_3 &= \varepsilon_{33}, \\ \varepsilon_4 &= 2\varepsilon_{23} = 2\varepsilon_{32}, & \varepsilon_5 &= 2\varepsilon_{31} = 2\varepsilon_{13}, & \varepsilon_6 &= 2\varepsilon_{12} = 2\varepsilon_{21}, \end{aligned}$$

$$(3.12) \quad \begin{aligned} c_{11} &= c_{1111} = c_{2222}, & c_{12} &= c_{1122}, & c_{13} &= c_{1133} = c_{2233}, \\ c_{33} &= c_{3333} & c_{44} &= c_{2323} = c_{3131}, & c_{66} &= c_{1212} = \frac{1}{2}(c_{11} - c_{12}), \end{aligned}$$

$$(3.13) \quad e_{15} = e_{131} = e_{223}, \quad e_{31} = e_{311} = e_{322}, \quad e_{33} = e_{333}.$$

3.2. Computational model

The three-dimensional finite element model of the piezoelectric transformer is shown in Fig. 3. A rectangular Cartesian coordinate system (x, y, z) is used. Two electrodes with length l and width $2w$ lie in the surfaces $z = \pm h$ of the input part, and an electrode of length $2w$ and width $2h$ is attached to the surface $x = l$ of the output part. The electric potential on the electrode surface $(-l \leq x \leq 0, |y| \leq w, z = h)$ equals the applied AC voltage, $\phi = V(t) = V_0 \exp(i\omega t)$ for Cases a and c; ω is angular frequency ($=2\pi f$ where f is frequency in Hertz). The system of Case c is also loaded by the resistance R and capacitance C .

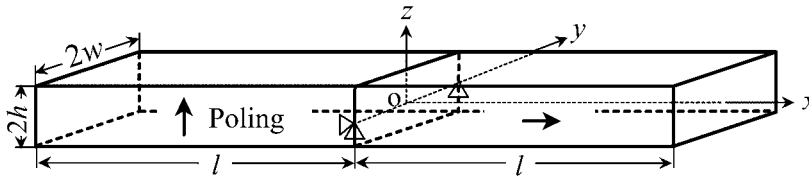


FIG. 3. Scheme of finite element model.

The electrode surface ($-l \leq x \leq 0$, $|y| \leq w$, $z = -h$) is connected to the ground, so that $\phi = 0$. For Case b, the electric potential on the electrode surface ($x = l$, $|y| \leq w$, $|z| \leq h$) equals the applied AC voltage $\phi = V(t) = V_0 \exp(i\omega t)$, and the electric potential is equal to zero on the surfaces ($-l \leq x \leq 0$, $|y| \leq w$, $z = \pm h$). The electrode layers are not incorporated into the model.

Mechanical boundary conditions are given by

$$(3.14) \quad \begin{aligned} \sigma_{xx}(\pm l, y, z) &= 0 & (|y| \leq w, |z| \leq h), \\ \sigma_{xy}(\pm l, y, z) &= 0 & (|y| \leq w, |z| \leq h), \\ \sigma_{xz}(\pm l, y, z) &= 0 & (|y| \leq w, |z| \leq h), \end{aligned}$$

$$(3.15) \quad \begin{aligned} \sigma_{yy}(x, w, z) &= 0 & (|x| \leq l, |z| \leq h), \\ \sigma_{yx}(x, w, z) &= 0 & (|x| \leq l, |z| \leq h), \\ u_z(0, w, 0) &= 0, \\ \sigma_{yz}(x, w, z) &= 0 & (0 < |x| \leq l, 0 < |z| \leq h), \end{aligned}$$

$$(3.16) \quad \begin{aligned} \sigma_{yy}(x, -w, z) &= 0 & (|x| \leq l, |z| \leq h), \\ u_x(0, -w, 0) &= 0, \\ \sigma_{yx}(x, -w, z) &= 0 & (0 < |x| \leq l, 0 < |z| \leq h), \\ u_z(0, -w, 0) &= 0, \\ \sigma_{yz}(x, -w, z) &= 0 & (0 < |x| \leq l, 0 < |z| \leq h), \end{aligned}$$

$$(3.17) \quad \begin{aligned} \sigma_{zz}(x, y, \pm h) &= 0 & (|x| \leq l, |y| \leq w), \\ \sigma_{zx}(x, y, \pm h) &= 0 & (|x| \leq l, |y| \leq w), \\ \sigma_{zy}(x, y, \pm h) &= 0 & (|x| \leq l, |y| \leq w). \end{aligned}$$

Electrical boundary conditions are summarized below.

For Case a

$$(3.18) \quad \begin{aligned} D_x(\pm l, y, z) &= 0 & (|y| \leq w, |z| \leq h), \\ D_y(x, \pm w, z) &= 0 & (|x| \leq l, |z| \leq h), \\ \phi(x, y, h) &= V_0 \exp(i\omega t) & (-l \leq x < 0, |y| \leq w), \\ \phi(x, y, -h) &= 0 & (-l \leq x < 0, |y| \leq w), \\ D_z(x, y, \pm h) &= 0 & (0 \leq x \leq l, |y| \leq w). \end{aligned}$$

For Case b

$$\begin{aligned}
 \phi(l, y, z) &= V_0 \exp(i\omega t) && (|y| \leq w, |z| \leq h), \\
 D_x(-l, y, z) &= 0 && (|y| \leq w, |z| \leq h), \\
 (3.19) \quad D_y(x, \pm w, z) &= 0 && (|x| \leq l, |z| \leq h), \\
 \phi(x, y, \pm h) &= 0 && (-l \leq x < 0, |y| \leq w), \\
 D_z(x, y, \pm h) &= 0 && (0 \leq x \leq l, |y| \leq w).
 \end{aligned}$$

For Case c

$$\begin{aligned}
 \phi(l, y, z) &= 4i\omega D_x(l, y, z)wh\{R^2C^2/(R^2 + C^2)\}^{1/2} \\
 &&& (|y| \leq w, |z| \leq h), \\
 D_x(-l, y, z) &= 0 && (|y| \leq w, |z| \leq h), \\
 D_y(x, \pm w, z) &= 0 && (|x| \leq l, |z| \leq h), \\
 (3.20) \quad \phi(x, y, h) &= V_0 \exp(i\omega t) && (-l \leq x < 0, |y| \leq w), \\
 \phi(x, y, -h) &= 0 && (-l \leq x < 0, |y| \leq w), \\
 D_z(x, y, \pm h) &= 0 && (0 \leq x \leq l, |y| \leq w).
 \end{aligned}$$

Calculations of impedance and phase for Cases a and b require the calculation of the ratio of the AC voltage $V(t)$ of the system to an alternating current $I(t)$. The impedance Z is expressed as

$$(3.21) \quad Z = \frac{V(t)}{I(t)} = |Z|e^{i\varphi}$$

where $|Z|$ is the impedance magnitude and φ is the phase difference between the voltage and current. The alternating current $I(t)$ is obtained as

$$(3.22) \quad I(t) = \begin{cases} i\omega \int_{-w}^w \int_{-l}^0 D_z(x, y, h) dx dy & \text{(Case a),} \\ i\omega \int_{-h}^h \int_{-w}^w D_x(l, y, z) dy dz & \text{(Case b).} \end{cases}$$

ANSYS elements SOLID5 and electrical circuit elements CIRCU124 were used in the analysis. SOLID5 has a three-dimensional piezoelectric and structural field capability. The element has eight nodes with up to six degrees of freedom at each node. On the other hand, CIRCU124 has a general circuit element applicable to circuit simulation. The element may also interface with piezoelectric finite elements to simulate coupled piezoelectric-circuit field interaction. The element has up to six nodes to define the circuit component and up to three degrees of freedom per node to model the circuit response.

4. Results and discussion

In order to confirm the results of the device simulation, the resonance characteristic of transformers is first measured and a quantitative comparison is made between measurements and finite element method (FEM). The impedance/phase-frequency spectra of the input part (Case a) are plotted in Fig. 4, in which both the measured and calculated data are shown. The impedance minimum peak corresponds to the resonance frequency, while the impedance maximum corresponds to antiresonance frequency. The measured (calculated) fundamental and second resonances are approximately $f_{r31-1} = 36(36)$ kHz and $f_{r31-2} = 71(74)$ kHz. It can be seen that the trend is sufficiently similar between analysis and experiment. Figure 5 shows the measured and calculated impedance/phase characteristics of the output part (Case b). The measured (calculated) fundamental and second resonance frequencies are about $f_{r31-1} = 33(32)$ kHz and $f_{r31-2} = 65(64)$ kHz, and agreement between analysis and experiment is fair.

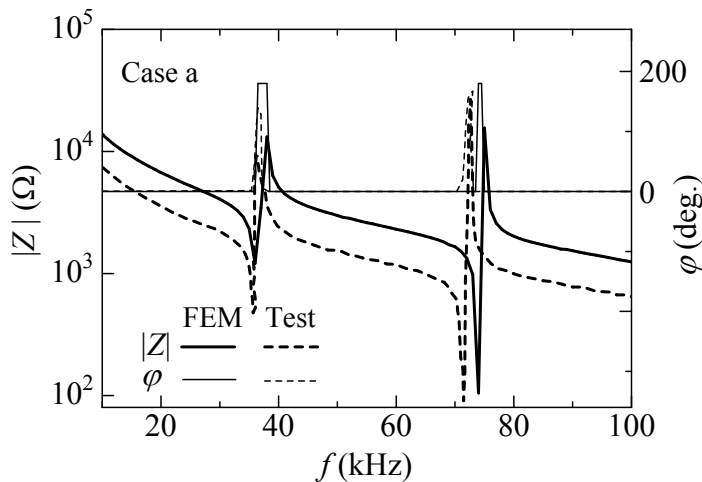


FIG. 4. Electrical impedance/phase spectra for the input part.

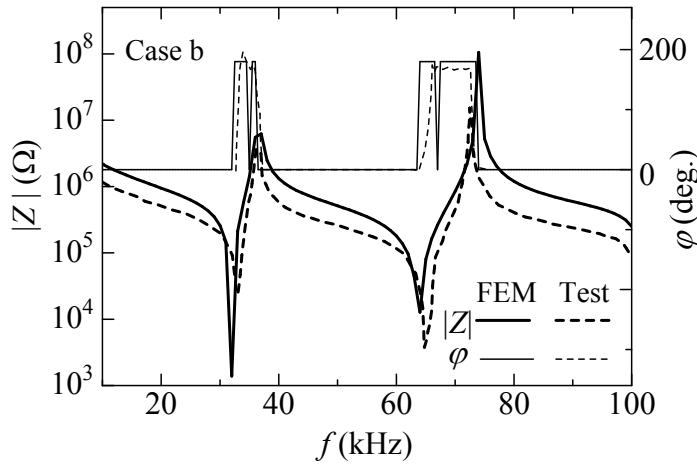


FIG. 5. Electrical impedance/phase spectra for the output part.

Figure 6 shows the output voltage V_{out} versus driving frequency f at input AC voltage $V_{in} = 10$ V and loads of $R = 1$ M Ω , $C = 160$ pF for Case c. Frequencies at which the maximum output voltages occur are approximately $f = 33, 65$ kHz, and they agree with the values of resonance frequencies of the output part (see Fig. 5). The finite element analysis predictions for the output voltage match all the experimental responses. Figure 7 shows the amplitude of normal stress σ_{xx} of the finite element solutions versus x at $y = 0$ mm, $z = 0$ mm for $V_{in} = 10$ V, $R = 1$ M Ω , $C = 160$ pF and $f = 33, 65$ kHz. The amplitude of normal stress σ_{xx} near the first resonance frequency remains smaller than that near the second resonance frequency. The amplitude of σ_{xx} in the output part is the largest on the vibration mode of the second mode (i.e., on $x = 12.5$ mm).

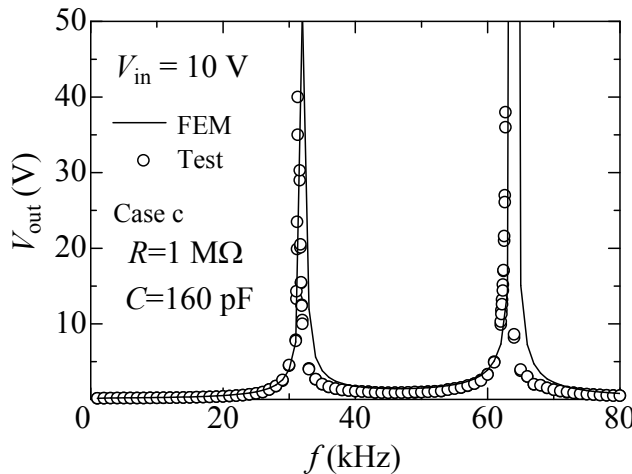


FIG. 6. Output voltage versus frequency for $R = 1$ M Ω and $C = 160$ pF.

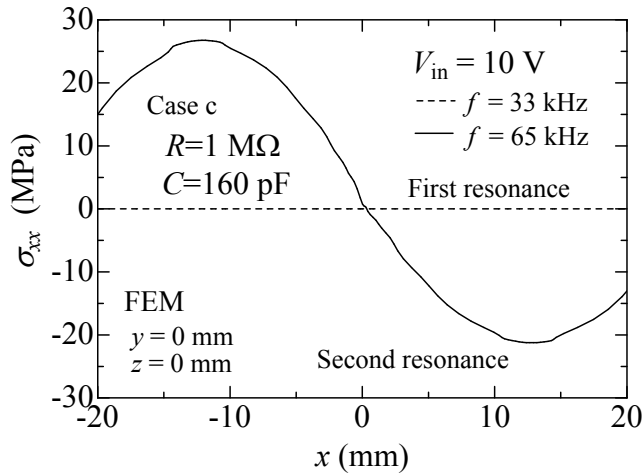


FIG. 7. Normal stress versus x for $R = 1 \text{ M}\Omega$ and $C = 160 \text{ pF}$.

Next, the output voltages and internal stresses obtained from the FEM are discussed in detail for the practical applications in liquid crystal display backlight inverters. Figure 8 shows the output voltage of the transformer before lighting the lamp versus the driving frequency at $V_{\text{in}} = 10 \text{ V}$ for $R = 1, 10 \text{ M}\Omega$ and $C = 0 \text{ pF}$ (Case c). The output voltage increases as the load resistance is increased from $1 \text{ M}\Omega$ to $10 \text{ M}\Omega$. Figure 9 shows the amplitude of normal stress σ_{xx} at $x = 12.5 \text{ mm}$, $y = 0 \text{ mm}$ and $z = 0 \text{ mm}$ under the same conditions shown in Fig. 8. The amplitude of normal stress also increases with the increase of load resistance. Figure 10 displays the output voltage of the transformer after

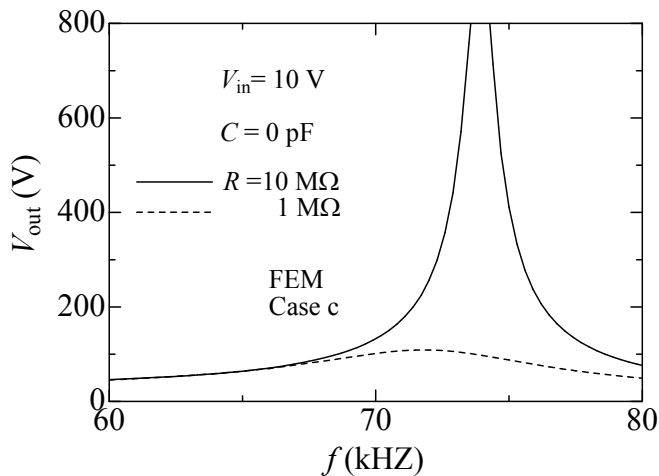


FIG. 8. Output voltage versus frequency for $R = 1, 10 \text{ M}\Omega$ and $C = 0 \text{ pF}$.

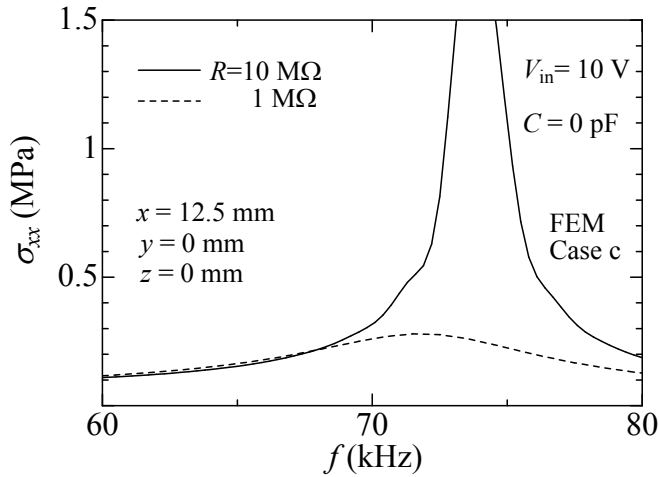


FIG. 9. Normal stress versus frequency for $R = 1, 10 \text{ M}\Omega$ and $C = 0 \text{ pF}$.

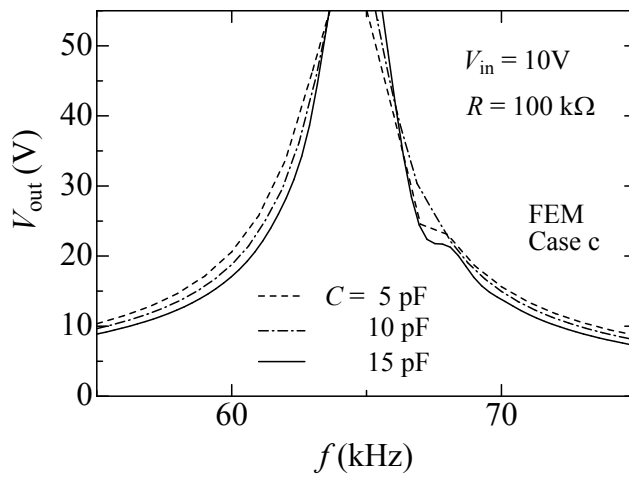


FIG. 10. Output voltage versus frequency for $R = 100 \text{ k}\Omega$ and $C = 5, 10, 15 \text{ pF}$.

lighting the lamp against the driving frequency at $V_{in} = 10 \text{ V}$ for $R = 100 \text{ k}\Omega$ and various values of capacitance (Case c). The capacitance has a small effect on the voltage gain. Figure 11 shows the amplitude of normal stress σ_{xx} versus C at $x = 12.5 \text{ mm}$, $y = 0 \text{ mm}$ and $z = 0 \text{ mm}$ for the steady state ($V_{in} = 10 \text{ V}$, $f = 65 \text{ kHz}$, and $R = 100 \text{ k}\Omega$). The results for $R = 500 \text{ k}\Omega$, $1 \text{ M}\Omega$ are also shown. The amplitude of normal stress is seen to increase with increasing the capacitance, depending on the load resistance.

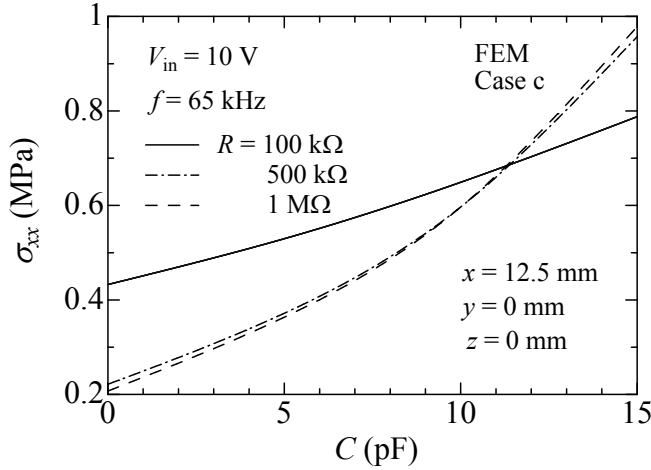


FIG. 11. Normal stress versus capacitance at 65 kHz for $R = 100, 500 \text{ k}\Omega, 1 \text{ M}\Omega$.

5. Conclusions

An experimental and numerical investigation was conducted to evaluate the high frequency characteristics of the piezoelectric transformers. The finite element model quantitatively predicted the electrical impedance/phase angle and voltage gain, and captured the dynamic phenomena related to macrospecimens. A higher voltage gain is attained with the increase of the load resistance. The voltage gain and internal electroelastic fields are strongly dependent on the load resistance and capacitance. This study is useful in designing piezoelectric transformers and in reducing the problem of failure that frequently occurs during service.

Acknowledgments

This work was supported by the Ministry of Education, Culture, Sports, Science and Technology of Japan under the Grant-in-Aid for Scientific Research (B).

References

1. S. MANUSPIYA, P. LAORATANAKUL and K. UCHINO, *Integration of a piezoelectric transformer and an ultrasonic motor*, *Ultrasonics*, **41**, 83–87, 2003.
2. N.Y. WONG, Y. ZHANG, H.L.W. CHAN and C.L. CHOY, *A bilayer piezoelectric transformer operating in a bending vibration mode*, *Mater. Sci. Eng. B*, **99**, 164–167, 2003.

3. L. HWANG, J. YOO, E. JANG, D. OH, Y. JEONG, I. AHN and M. CHO, *Fabrication and characteristics of PDA LCD backlight driving circuits using piezoelectric transformer*, Sens. Actuators A, **115**, 73–78, 2004.
4. V. L. KARLASH, *Electroelastic vibrations and transformation ratio of a planar piezoceramic transformer*, J. Sound Vib., **277**, 353–367, 2004.
5. F. NARITA, S. LIN and Y. SHINDO, *Electroelastic fracture mechanics analysis of central active piezoelectric transformer*, Eur. J. Mech. A, **24**, 377–392, 2005.
6. Y. SHINDO, H. MURAKAMI, K. HIRIGUCHI and F. NARITA, *Evaluation of electric fracture properties of piezoelectric ceramics using the finite element and single-edge precracked-beam methods*, J. Am. Ceram. Soc., **85**, 1243–1248, 2002.
7. Y. SHINDO, F. NARITA and M. MIKAMI, *Double torsion testing and finite element analysis for determining the electric fracture properties of piezoelectric ceramics*, J. Appl. Phys., **97**, 114109, 2005.
8. M. YOSHIDA, F. NARITA, Y. SHINDO, M. KARAIWA and K. HIRIGUCHI, *Electroelastic field concentration by circular electrodes in piezoelectric ceramics*, Smart Mater. Struct., **12**, 972–978, 2003.
9. Y. SHINDO, M. YOSHIDA, F. NARITA and K. HIRIGUCHI, *Electroelastic field concentrations ahead of electrodes in multilayer piezoelectric actuators: experiment and finite element simulation*, J. Mech. Phys. Solids, **52**, 1109–1124, 2004.
10. F. NARITA, Y. SHINDO and M. MIKAMI, *Analytical and experimental study of nonlinear bending response and domain wall motion in piezoelectric laminated actuators under ac electric fields*, Acta Mater., **53**, 4523–4529, 2005.

Received July 14, 2006; revised version October 10, 2006.
